Monthly Notices
of the
ROYAL ASTRONOMICAL SOCIETY

MNRAS **472,** 1361–1371 (2017)
Advance Access publication 2017 July 22

doi:10.1093/mnras/stx1867

Monte Carlo simulations of thermal comptonization process in a two-component advective flow around a neutron star

Ayan Bhattacharjee[1]★ and Sandip K. Chakrabarti[1,2]★

[1]*S. N. Bose National Centre for Basic Sciences, Block -JD, Sector -3, Salt Lake, Kolkata 700106, India*
[2]*Indian Center for Space Physics, 43 Chalantika, Garia St. Road, Kolkata 700084, India*

Accepted 2017 July 20. Received 2017 July 19; in original form 2017 February 20

ABSTRACT

We explore spectral properties of a two-component advective flow around a neutron star. We compute the effects of thermal Comptonization of soft photons emitted from a Keplerian disc and the boundary layer of the neutron star by the post-shock region of a sub-Keplerian flow, formed due to the centrifugal barrier. The shock location X_s is also the inner edge of the Keplerian disc. We compute a series of realistic spectra assuming a set of electron temperatures of the post-shock region T_{CE}, the temperature of the Normal BOundary Layer (NBOL) T_{NS} of the neutron star and the shock location X_s. These parameters depend on the disc and halo accretion rates ($\dot{m}_d$ and $\dot{m}_h$, respectively) that control the resultant spectra. We find that the spectrum becomes harder when $\dot{m}_h$ is increased. The spectrum is controlled strongly by T_{NS} due to its proximity to the Comptonizing cloud since photons emitted from the NBOL cool down the post-shock region very effectively. We also show the evidence of spectral hardening as the inclination angle of the disc is increased.

Key words: accretion, accretion discs – radiation: dynamics – scattering – shock waves – stars: neutron – X-rays: binaries.

1 INTRODUCTION

The theoretical modelling and spectral studies of compact objects go hand in hand in understanding the accretion processes. In the past twenty five years, theoretical studies of accretion on to black holes have reached a very satisfactory stage (for a recent review, see Chakrabarti 2016) where it was shown that multiple aspects of observations of a large number of objects can be explained within a single framework. However, similar studies for a neutron star (NS) accretion have not been done, primarily because it is inherently more complex. First, an NS can have a magnetic field that interacts with the accretion flow. If it is strong enough, it can block direct accretion and the flow then approaches the star through the poles. Secondly, it has a hard surface that can have a range of temperatures thereby posing a difficult boundary value problem. The matter has to stop on the surface in the corotating frame with the star. In other words, independent of its past history, its final leg of journey must be sub-sonic and may form a boundary layer. In contrast, a black hole accretion flow always enters through the horizon with a velocity of light and is always supersonic. Another important difference is that while for a black hole accretion, there could be one single centrifugal barrier supported shock in a transonic flow, in an NS, there could be two shocks, one at a similar distance (in dimensionless unit) as in a black hole accretion and the other one right outside the hard surface (Chakrabarti 1989; Chakrabarti & Sahu 1997) of the star formed due to the boundary condition. The outer one is known as the CENtrifugal barrier supported BOundary Layer (CENBOL) and the inner one may be called the Normal BOundary Layer (NBOL). Thus, in a black hole accretion, energy is dissipated at the CENBOL and jets/outflows are produced there as well. In an NS accretion, both the boundary layers can take part in dissipating the compressional heat of thermal electrons. So the spectral properties are more complex. One interesting common theme, as far as the mathematical properties go, is that both the flows are sub-Keplerian at the very inner edge: For NS the sub-Keplerian nature is required to adjust with the sub-Keplerian rotation of the surface; while for black holes, the passage through the inner sonic point ensures that the flow is sub-Keplerian. Thus, a thorough fundamental understanding of the accretion flow is important. This paper is the first study to explore these aspects.

The most complete theoretical solution in the presence of advection, radiative transfer and heating is a transonic or advective flow (Chakrabarti 1990; Chakrabarti 1996, hereafter C96), which self-consistently passes through one or more sonic points. It was shown that in the absence of a significant viscosity, the flow will have a steady or oscillating shock but it would disappear when viscosity is high and the flow would be similar to a standard Shakura & Sunyaev (1973 , hereafter SS73) disc. Chakrabarti & Titarchuk (1995, hereafter CT95), used the two-component advective flow (TCAF) solution to show that spectral states of black holes could be understood by changes in the two independent accretion rates. Indeed,

★ E-mail: ayan12@bose.res.in (AB); chakraba@bose.res.in (SKC)

numerical simulations of Giri & Chakrabarti (2013) and Giri, Garain & Chakrabarti (2015) show that the two components are naturally produced when there is a vertical gradient of viscosity parameter. It was shown that when the viscosity parameter is higher than the critical value in the equatorial region, a standard Keplerian disc (KD) is formed flanked vertically by an advective sub-Keplerian halo as already envisaged before (C96).

Historically, the explanation of soft state spectra of NSs demanded the presence of a blackbody emission from the boundary layer of an NS (Mitsuda et al. 1984). For the harder states with a power-law tail in the energy spectrum, the need of Compton scattering became evident (White et al. 1986; Mitsuda et al. 1989). The difference between these two models was that while the former assumed a cooler boundary layer, the latter assumed a hotter one, compared to the accretion disc. Sunyaev and his collaborators (Inogamov & Sunyaev 1999, hereafter IS99; Popham & Sunyaev 2001, hereafter PS01; Gilfanov & Sunyaev 2014 , hereafter GS14) assume that the KD reaches all the way to the NS and is connected with the boundary layer where the thickness increases due to higher temperature. Most of these studies were done to address the soft state spectra of NSs. The state transition of NSs in Low Mass X-ray Binaries (LMXBs), presented another problem. The fact that disc accretion rate was not the single factor that controlled the size or temperature of the Compton cloud, used to model the hard state spectra, lead to the conclusion that some unknown parameter, related to the truncation radius of the disc, is responsible for the hard X-ray tail (Barret 2001; Barret & Olive 2002; Di Salvo & Stella 2002). Paizis et al. (2006) found a systematic positive correlation between the X-ray hard tail and the radio luminosity, inferring that the Compton cloud might serve as the base of radio jets (see Chakrabarti 2016, and references therein). Recent phenomenological works places a transition layer (TL) or Compton cloud between the KD and the boundary layer (Farinelli et al. 2008; Titarchuk, Seifina & Shrader 2014, hereafter TSS14). It has been argued in the past (Chakrabarti 1989; C96; Chakrabarti & Sahu 1997) that while in black hole accretion, passing of the flow through the inner sonic point ensures that the flow becomes sub-Keplerian just outside the horizon, in the case of NSs, the Keplerian flow velocity must slow down to match with the sub-Keplerian surface velocity. Numerical simulations clearly showed that jumping from a KD to a sub-Keplerian disc is mediated by a super-Keplerian region (Chakrabarti & Molteni 1995). In Titarchuk, Lapidus & Muslimov (1998, hereafter TLM98), a super-Keplerian TL was invoked to explain the kHz quasi-periodic oscillations (QPOs) and in TSS14 the TL was expanded several fold to explain the spectral properties. In reality, there are two such layers simultaneously present in an NS accretion: One is similar to the NBOL and the other is similar to the CENBOL in a black hole accretion (CT95). In a black hole accretion, only CENBOL is present. All these approaches clearly point to the existence of a CENBOL type hot electron reservoir, which naturally occurred in black hole accretion, confirming Chakrabarti & Sahu (1997) conclusions that the solutions of the transonic flows are modified only in the last few Schwarzschild radii as per the boundary condition of the gravitating object.

Monte Carlo simulations are essential in generating and understanding spectra emergent from highly non-local processes such as Comptonization. Toy models were made of spherical Compton clouds of constant temperature and optical depth, surrounding a weakly magnetic NS to generate hard X-ray tails (Seon et al. 1994). In case of NSs with strong magnetic fields ($B \sim 10^{10}$–10^{12} G), matter lands at the poles through the accretion column and the use of such a geometry leads to the successful explanation of spectral properties (Odaka et al. 2013, 2014) in certain cases. Although these studies provide some answers, so far, the spectral fitting carried out were based on phenomenological models that used an arbitrarily placed Compton cloud. TLM98 explained high-frequency QPOs considering a TL, and an extended TL was used to explain spectra using COMPTT and COMPTB models. Out of the two COMPTB components used, the one corresponding to Comptonization of NSs surface photons, showed a saturation in COMPTB models spectral index (Farinelli & Titarchuk 2011, hereafter FT11). The 'Spectral slope/index' in the context of COMPTB model, refers to α which is the slope of Comptonized component of the spectrum ($=\Gamma - 1$, the photon index). In this paper, we uniformly use the actual slope of the linear region of the spectrum (which includes both the primary and Comptonized photons) in log–log scale. Thus, the two terms do not represent the same quantity. Many NS LMXBs are studied using this framework, such as 4U 1728-34 (Seifina et al. 2011), GX 3+1 (Seifina & Titarchuk 2012, hereafter ST12), GX 339+0 (Seifina, Titarchuk & Frontera 2013, hereafter STF13), 4U 1820-30 (Titarchuk, Seifina & Frontera 2013, hereafter TSF13), Scorpius X-1 (TSS14), 4U 1705-44 (Seifina et al. 2015, hereafter STSS15), etc. Recently, the HMXB 4U 1700-37 has also been examined using the same model (Seifina, Titarchuk & Shaposhnikov 2016, hereafter STS16). This useful model to fit the spectra of NSs give the average temperature of the Compton cloud placed in between the disc and the NS surface, unlike what the TL used just outside the star. With an independent advective flow as in TCAF, the phenomenological Compton cloud is naturally explained without having to modify the earlier models drastically. Indeed, since the flow at the outer edge of the disc has little knowledge of the nature of the compact source, except near the innermost boundary, the overall flow configuration is not expected to be very different, especially when the magnetic field is weak ($<10^8$ G). The gravity simply lets the advective matter to fall almost freely till the surface of the star is hit.

In this paper, we study spectral properties of an NS in the presence of TCAF, which has a CENBOL as well as the NBOL of the star. A preliminary report has been presented in Bhattacharjee, Chakrabarti & Banerjee (2016). We use the size of the CENBOL (X_s), accretion rates of the KD and the sub-Keplerian halo as the free parameters. Additional parameters in the present context are the mass of the NS and the temperature of the NBOL. In the next section, we present a brief introduction to the TCAF solution around a black hole and how the solution is modified when the black hole is replaced by an NS. In Section 3, we describe the system in detail and define the properties of the NBOL, CENBOL and the KD. In Section 4, we describe, in brief, the Monte Carlo simulation procedure used in thermal Comptonization. The resultant spectra of the flow as a function of the flow parameters are given in Section 5. Finally, in Section 6, we give our concluding remarks.

2 TWO-COMPONENT FLOWS AROUND NSs

It is well known that the spectral and timing properties of a black hole cannot be explained by a standard KD alone (Sunyaev & Truemper 1979; Sunyaev & Titarchuk 1980, 1985; Chakrabarti & Wiita 1993; Haardt & Maraschi 1993; Chakrabarti & Titarchuk 1995; Chakrabarti 1997; Zdziarski 2003). A spectrum clearly has a thermal component resembling of a multicolour blackbody radiation. However, the other component is similar to a power-law component, which is produced by inverse Comptonization of the thermal or non-thermal electrons (Sunyaev & Titarchuk 1980, 1985). There are many models in the literature that present possible scenarios of how the electron cloud might be

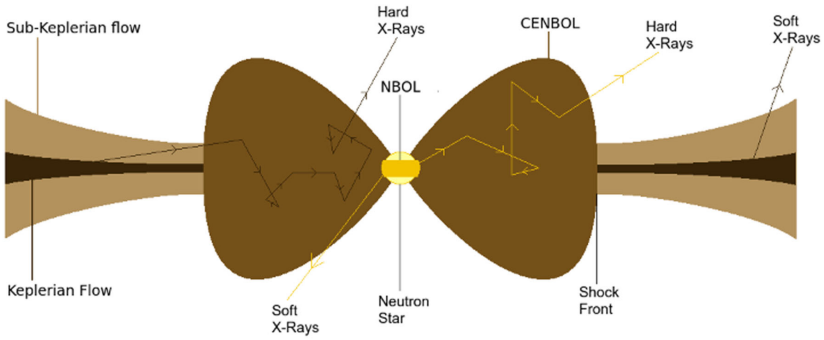

Figure 1. A schematic diagram of the two-component advective flow (TCAF) around an NS. The KD and the boundary layer on the surface of the NS (NBOL) emit soft blackbody photons, which are scattered by the hot electrons in the centrifugal pressure supported boundary layer or CENBOL.

produced. However, there is a unique self-consistent solution, namely, the transonic flow solution based TCAF that addresses all the aspects of spectral and temporal properties at the same time. In this scenario, a CENBOL is produced very close to a compact object in the low-viscosity advection component. The boundary of CENBOL is a shock transition which may or may not be stationary. The post-shock region is a natural reservoir of hot electrons. Higher viscosity flow component near the equatorial plane becomes a KD and emits a multicolour blackbody radiation, which are intercepted and re-radiated by the CENBOL to create the power law like component which normally has an exponential cut-off where recoil becomes important. When the shock oscillates due to resonance (Molteni, Sponholz & Chakrabarti 1996) or non-satisfaction of Rankine–Hugoniot condition (Ryu, Chakrabarti & Molteni 1997), the resulting hard X-ray intensity is modulated with the size of the CENBOL and manifest as the low-frequency quasi-Periodic oscillations (LFQPOs). The CENBOL is also the source of outflows and jets, in that, when the CENBOL is cooled down due to excessive soft photons, the jet itself also disappears. There are clear observational evidence of two-component advective flows in several black hole candidates (Smith et al. 2001; Smith, Heindl & Swank 2002; Debnath, Chakrabarti & Mondal 2013a; Mondal, Debnath and Chakrabarti, 2014; Dutta & Chakrabarti 2016).

Since the nature of the companion remains generally similar irrespective of whether the compact object is a black hole or an NS, it is natural that we invoke the TCAF solution for the NSs as well, specifically when the magnetic field is not very strong. However, in addition to the CENBOL, to satisfy the inner boundary condition, the flow would have an optically thick boundary layer of the NS, which would also emit a characteristic blackbody radiation. These photons would be inverse Comptonized by the electrons inside the CENBOL, cooling it down further and making the spectra softer. In presence of a stronger magnetic field, a hot corona is produced when matter proceeds to the magnetic poles of the NS. This is also the region of inverse Comptonization. However, discussion on this case will require inclusion of synchrotron radiation, which is beyond the scope of this paper. In our solution, the Compton cloud is always a very hot reservoir of electrons (as compared to the NBOL or the KD), unless it is cooled down by the disc and/or NBOL.

3 MONTE CARLO SIMULATION OF TCAF AROUND A NEUTRON STAR

3.1 Simulation setup

In earlier papers from our group, Monte Carlo simulation results of TCAFs around black holes were presented (Ghosh, Chakrabarti & Laurent 2009; Ghosh et al. 2010, hereafter GCL09 and GGCL10, respectively). In the present context, in addition to the components used earlier, we must include a boundary layer (NBOL) of the star that will emit a blackbody radiation. In Fig. 1, we present the flow configuration of our simulation. We also use a more realistic post-shock region or CENBOL, namely, one that resembles a thick accretion disc (Molteni, Lanzafame & Chakrabarti 1994). Since we are considering a stationary configuration, to begin with, we use the density and temperature distribution as specified by Chakrabarti (1985) inside a general relativistic model of the thick accretion disc.

The three components of our simulation configuration, namely, the boundary layer of the NS (NBOL), the Comptonizing cloud (CENBOL) and the KD are discussed below:

3.1.1 *Normal boundary layer*

It is a thermal blackbody radiation emitting region on the surface of the NS, that is symmetrically placed around the equatorial plane between the azimuthal angles $(90^\circ - \theta_*)$ *to* $(90^\circ + \theta_*)$, where θ_* is an angle that decides the thickness of the boundary layer. The mass of the star is kept constant at $M_{\rm NS} = 1.4\,{\rm M}_\odot$. The radius of the spherical NS is taken as $r_{\rm NS} = 3r_{\rm S}$, where $r_{\rm S} = \frac{2GM_{\rm NS}}{c^2}$ is the Schwarzschild radius of the NS. Here, c is the speed of light in vacuum. From previous works carried out by IS99 and GS14 the temperature of an accreting NS is reported to be around 1.4 keV in the soft states. For our cases, we set the maximum value of accretion rate to one Eddington rate and the corresponding temperature is set to $T_{\rm NS}^{\rm max} = 1.2$ keV. An empirical dependence on accretion rates is chosen based on the fact that emitted flux is proportional to the accretion rate, which is formulated as

$$T_{\rm NS} = T_{\rm NS}^{\rm max} \times (\dot{m}_{\rm d} + \dot{m}_{\rm h})^{1/4}\ {\rm keV}. \quad (1)$$

The flux density of photons emitted from the surface, corresponding to temperature T is calculated using (adopted from Garain, Ghosh & Chakrabarti 2014, hereafter GGC14):

$$n_\gamma = \left[\frac{4\pi}{c^2}\left(\frac{k_{\rm b}}{h}\right)^3 \times 1.202\,057\right] T^3\ {\rm cm}^{-2}\ {\rm s}^{-1}, \quad (2)$$

We follow the work of IS99, where it is reported that the angle $\theta_* \longrightarrow 90^\circ$, when $\dot{M} \longrightarrow \dot{M}_{\rm Edd}$. For our calculations, accretion rates are written in the units of $\dot{M}_{\rm Edd}$. So, to incorporate such an effect, we assume a simpler variation of θ_*, given by

$$\theta_* = \sin^{-1}(\dot{m}_{\rm d} + \dot{m}_{\rm h}), \qquad if\ (\dot{m}_{\rm d} + \dot{m}_{\rm h}) \leq 1. \quad (3)$$

The flux, however, is not a constant with respect to θ. It is believed that due to the meridional motion of the flow in the NBOL, radiation reaches a maximum flux near the angle θ_* (IS99). The effect of this is incorporated, at least qualitatively, by using a truncated double Gaussian distribution of photon flux where the peaks are located at $\theta_{\rm P}^{\pm}$. We took the 95 per cent of the θ_* as the location of the peaks, as this is not crucial to the net final spectrum, i.e.

$$\theta_{\rm P}^{\pm} = (90^{\circ} \pm 0.95 \times \theta_*). \tag{4}$$

The form of the distribution takes the form

$$f(\theta) = \exp(-(\theta - \theta_{\rm P}^{+})^2) + \exp(-(\theta - \theta_{\rm P}^{-})^2). \tag{5}$$

After calculating the total flux from the entire NBOL, we redistributed the photon numbers according to the double Gaussian profile $f(\theta)$ along θ so as to have a realistic injection of photons from the NBOL on to CENBOL.

3.1.2 CENBOL

The CENBOL is modelled in shape by the equipotential contours of a standard thick disc (Chakrabarti 1985; Chakrabarti, Jin & Arnett 1987; GCL09). The analytical forms of potential ϕ, adiabatic constant related to entropy K, density ρ and temperature $T_{\rm e}$ profiles are given below

$$\phi = \frac{\lambda^2}{2(r^2 - z^2)} - \frac{1}{2(r-1)} = \frac{\lambda^2}{2R^2} - \frac{1}{2(\sqrt{R^2+z^2}-1)}, \tag{6}$$

where λ is the specific angular momentum, R is the cylindrical radius, z is the vertical height, $r = \sqrt{R^2+z^2}$ is the radial distance and ϕ is the specific potential energy in units of c^2 (Chakrabarti 1985; GCL09).

The entropy ($K(\beta, \mu)$) is defined as (Chakrabarti 1985; GCL09)

$$K(\beta,\mu) = \left[\frac{3}{a}\frac{1-\beta}{\beta^4}\frac{(k_{\rm b})^4}{(\mu m_{\rm p})^4}\right]^{1/3} \ {\rm cm}^3\ {\rm g}^{-1/3}\ {\rm s}^{-2}, \tag{7}$$

where μ is the mean molecular weight, a is the Stefan's radiation density constant, β is the ratio of gas pressure and total pressure, $k_{\rm b}$ is the Boltzmann constant and $m_{\rm p}$ is the mass of the proton.

The density ρ is then written as (adapted from GCL09; Chakrabarti 1985)

$$\rho(r,z) = C_\rho \times \left[\frac{\phi(r,z)}{n\gamma K}\right]^n \ {\rm g\ cm}^{-3}, \tag{8}$$

where n is the polytropic index and γ is the adiabatic index.

The temperature $T_{\rm e}$ can also be written as (adapted from GCL09; Chakrabarti 1985)

$$T_{\rm e}(r,z) = C_{\rm T} \times \left[\frac{\beta \mu m_{\rm p} K}{k_{\rm b}}\right] \rho^{1/3}\ {\rm K}. \tag{9}$$

For our calculations, $\lambda = 1.9$, $\beta = 0.5$ and $n = 3.0$ and the centre of the thick disc is at $\sim 4.25 r_{\rm S}$. We did not modify the entropy by tuning β, but kept it constant at 0.5 throughout. Here, $C_{\rm T}$ is a constant introduced to supply the central temperature as a parameter. In order to obtain the spectra relevant to the observed ones, we restrict the central temperature of the CENBOL to the range obtained so far by previous observational fits (between 3 and 25 keV). From the observational and theoretical studies of accretion on to black holes, it is well known that with increasing disc accretion rate, CENBOL would be cooled down and become smaller in size. This is regularly observed in outbursting candidates, such as GRO J1655-40, GX339-4, H1743-322, MAXI J1836-194, MAXI J1543-564, etc. (Debnath et al. 2008; Debnath, Chakrabarti & Nandi 2010; Debnath, Chakrabarti & Nandi 2013b; Mondal et al. 2014; Jana et al. 2016; Chatterjee et al. 2016; Molla et al. 2016, 2017; Mondal, Chakrabarti & Debnath 2016). This happens because the photon flux from the disc increases with $\dot{m}_{\rm d}$. This soft radiation cools down the CENBOL and the shock condition (balancing of pressure on both sides of the shock) is satisfied at a smaller value of shock location. In order to incorporate this, we use the scaling behaviour of the CENBOL with central temperature. For our case, a reference is set for $\dot{m}_{\rm d} = 0.2\,\dot{M}_{\rm EDD}$, $T_{\rm CE} = 10$ keV and $X_{\rm s} = 30 r_{\rm S}$. The density is modified by the constant C_ρ, which is determined self-consistently from the strong shock condition of a hybrid 1.5 dimensional advective flow solution (Chakrabarti 1989). The disc and halo accretion rates ($\dot{m}_{\rm d}$ and $\dot{m}_{\rm h}$, respectively), the shock location ($X_{\rm s}$) and the compression ratio ($R_{\rm comp}$) determine the density at the post-shock region. The pre-shock flow is assumed to have a velocity, $v_{\rm R} \sim R^{-1/2}$ since the lower angular momentum flow would be quasi-spherical. In the post-shock region, the matter initially slows down and gradually picks up its speed. For a black hole, matter becomes supersonic before crossing the horizon. In case of NSs, the hard surface and the flow pressure force the matter to slow down just before reaching the surface.

The parameters we use in our simulations are given in Table 1. There are altogether nine cases divided into three groups with different disc accretion rates ($\dot{m}_{\rm d}$) and the central temperatures ($T_{\rm CE}$). Once we normalize the outer edge of the CENBOL at $X_{\rm s} = 30.0$ for cases C4-C6, the outer edge changes following constant temperature contours and the corresponding $X_{\rm s}$ are given in the Table. For each ($\dot{m}_{\rm d}$, $T_{\rm CE}$) pair, we change the halo rate $\dot{m}_{\rm h}$. Since the matter density inside the CENBOL is decided by the sum of the two rates, the number density of electrons at the centre of CENBOL also changes. The values of $T_{\rm NS}$, θ_* and $T_{\rm e}(\tau_0)$ are obtained from equations (1), (3) and (13), respectively.

In Fig. 2, we present the temperature contours corresponding to $C3$. The contours show that a CENBOL is essentially a toroidal star with highest density and temperature at the 'centre' (which is actually a ring around the NS). The vertical colour bar shows the temperatures in dimensionless unit.

For a cylinder of half height $h_{\rm s}$ and radius $X_{\rm s}$, we have the accretion rate $\dot{m}_{\rm tot}$

$$\dot{m}_{\rm tot} = (\dot{m}_{\rm d} + \dot{m}_{\rm h}) = 4\pi X_{\rm s} h_{\rm s} \rho_+ v_+. \tag{10}$$

The density at the equatorial plane of the post-shock flow is written as (from equation 10)

$$\rho_+ = \frac{(\dot{m}_{\rm d} + \dot{m}_{\rm h}) R_{\rm comp}}{4\pi h_{\rm s}\sqrt{X_{\rm s}}}. \tag{11}$$

In writing equations (10) and (11), $R_{\rm comp}$ used represents the shock compression ratio. We have assumed a strong shock condition for our calculation and set $R_{\rm comp} = 4$ for that purpose, throughout the simulations. As there is effectively optically thin matter outside CENBOL, we set the density outside to 0 except on the equatorial plane where there is a KD.

$$\rho(r,z) = 0, \quad \textit{if } \phi(r,z) > \phi(X_{\rm s}, 0). \tag{12}$$

The effective temperature is calculated by transforming from coordinate space into τ space and then averaging over all values of $T_{\rm e}(\tau)$. We followed the method of CT95 for this purpose.

$$T_{\rm e}(\tau_0) = \frac{\int_0^{\tau_0} T_{\rm e}(\tau) g^2(\tau)(\tau - \tau_0)^2 {\rm d}\tau}{\int_0^{\tau_0} g^2(\tau)(\tau - \tau_0)^2 {\rm d}\tau}, \ \text{where} \tag{13}$$

Table 1. Set of parameters chosen for the simulations. Disc accretion rate ($\dot{m}_{\rm d}$) and halo accretion rate ($\dot{m}_{\rm h}$) are varied independently. Temperatures are from typical observational ranges and consistent with high disc accretion rates, leading to lower temperatures of CENBOL. Shock locations ($X_{\rm s}$) are chosen accordingly. NSs (NBOL) temperature ($T_{\rm NS}$), θ_* and central number density $n_{\rm ce}$ are derived using empirical rules given in the text.

ID	$\dot{m}_{\rm d}$ ($\dot{M}_{\rm EDD}$)	$\dot{m}_{\rm h}$ ($\dot{M}_{\rm EDD}$)	$X_{\rm s}$ ($r_{\rm S}$)	$T_{\rm CE}$ (keV)	$n_{\rm ce}$ ($\times 10^{18}$)	$T_{\rm NS}$ (keV)	θ_* (°)	$T_{\rm e}(\tau_0)$ (keV)
C1	0.1	0.1	46.8	25.0	1.772	0.802	11.52	22.062
C2	0.1	0.2	46.8	25.0	2.658	0.888	17.48	22.062
C3	0.1	0.5	46.8	25.0	5.317	1.056	36.90	22.062
C4	0.2	0.1	30.0	10.0	1.515	0.888	17.48	8.909
C5	0.2	0.2	30.0	10.0	2.020	0.954	23.61	8.909
C6	0.2	0.5	30.0	10.0	3.535	1.098	44.40	8.909
C7	0.5	0.1	21.8	3.0	2.100	1.056	36.90	2.705
C8	0.5	0.2	21.8	3.0	2.450	1.098	44.40	2.705
C9	0.5	0.5	21.8	3.0	3.500	1.200	90.00	2.705

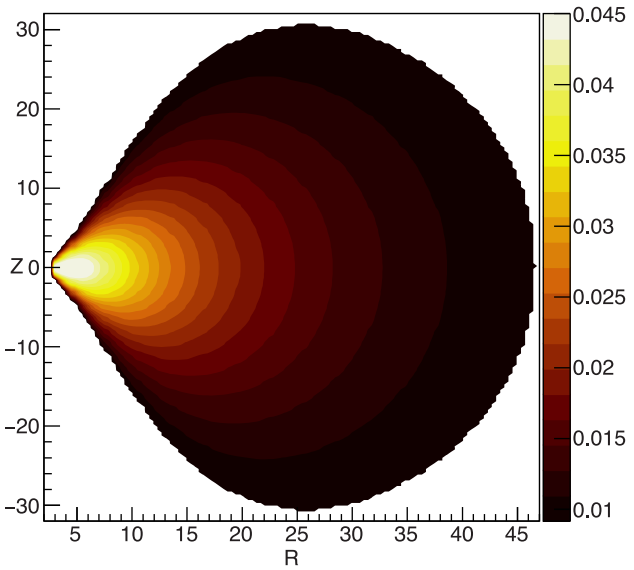

Figure 2. The temperature contours used for the simulation (for $\dot{m}_{\rm d} = 0.1$, $T_{\rm CE} = 25.0\,{\rm keV}$, $X_{\rm s} = 46.8 r_{\rm S}$. The temperatures are written in dimensionless unit ($kT_{\rm e}/mc^2$). This profile, symmetric with respect to z-axis, is used to get the values of temperatures at different points of CENBOL.

$$g(\tau) = \left(1 - \frac{3}{2}{\rm e}^{-(\tau_0+2)}\right) \cos\frac{\pi}{2}\left(1 - \frac{\tau}{\tau_0}\right) + \frac{3}{2}{\rm e}^{-(\tau_0+2)}. \quad (14)$$

Here, the integration is carried out along the equatorial plane (along R-direction).

3.1.3 Keplerian disc (KD)

A dense region of geometrically thin and optically thick disc extends outwards from the outer edge of CENBOL ($X_{\rm s}$). The outer edge of the disc is set at $R_{\rm out} = 200 r_{\rm S}$ for simplicity. The standard Shakura–Sunyaev disc (SS73) is used to determine the flux and height of disc as a function of radial distance in between $X_{\rm s}$ and $R_{\rm out}$. This acts as a secondary source of blackbody photons. Here, ${\rm d}r = 0.5\,r_{\rm S}$, $\dot{M}_{17}$ is the disc accretion rate in the units of 10^{17} gm s^{-1}. The radial distance r is measured in the units of $r_{\rm S}$. The injected energy flux is given by (SS73; GCL09)

$$F(r) = 5 \times 10^{26} (M_{\rm NS})^{-2} \dot{M}_{17} (2r)^{-3} \left[1 - \sqrt{\frac{3}{r}}\right] \ {\rm erg\ cm^{-2}\ s^{-1}}. \quad (15)$$

From which, the effective temperature ($T(r) = (F(r)/\sigma)^{1/4}$) and height of the disc is determined as (adopted from GCL09)

$$T(r) \approx 5 \times 10^7 (M_{\rm NS})^{-1/2} \dot{M}_{17}^{1/4} (2r)^{-3/4} \left[1 - \sqrt{\frac{3}{r}}\right]^{1/4} {\rm K}, \quad (16)$$

$$H(r) = 10^5 \dot{M}_{17} \left[1 - \sqrt{\frac{3}{r}}\right] {\rm cm}. \quad (17)$$

For our case, every cylindrical shell between r and $r + \delta r$ of height $H(r)$, emits a total ${\rm d}N(r)$ number of photons per second (GGC14) from its top and bottom surfaces, where

$${\rm d}N(r) \approx 2\pi r \delta r n_\gamma(r). \quad (18)$$

For computational purposes, we chose packets of photon instead of individual photons, in such a way that, effective ${\rm d}N(r) \sim 10^5$, which is required for a good statistics.

4 SCATTERING PROCESS

We adopt the method followed by Pozdnyakov, Sobol & Sunyaev (1983, hereafter PSS83) to model the thermal Compton scattering process.

4.1 Radiative processes

We simulate thermal Compton scattering phenomenon between the soft photons emitted by the KD (or, the NBOL, the boundary layer of the NS) and the hot electrons in the post-shock region (CENBOL), using a Monte Carlo code. Photons from the KD and the boundary layer are modelled using Planck's distribution formula for blackbody radiation. The radial temperature distribution for KD $T(r)$ is used as above. For the NS, the value ($T_{\rm NS}$) is kept constant throughout the simulation. In both the cases, the number density of photons ($n_\gamma(E)$) having an energy between E and $E + {\rm d}E$ is expressed by (PSS83)

$$n_\gamma(E) = \frac{1}{2\zeta(3)} b^3 E^2 ({\rm e}^{bE} - 1)^{-1}, \quad (19)$$

where $b = 1/kT$. Here, $T = T(r)$ for KD and $T = T_{\rm NS}$ for NS. The zeta function, $\zeta(3) = \sum_1^\infty l^{-3} = 1.202$.

For every packet of photon, we start the simulation by determining the local normal at the randomly chosen position on the (i) NBOL or the (ii) KD. Then, a random direction ($\theta_{\rm r}$) is chosen with respect to the local normal, with the probability density $\cos(\theta_r)$.

We also assign a random critical optical depth τ_c. During the photons' motion, we calculate τ by summing over $d\tau$ to check if it has crossed τ_c or not. Here, $d\tau = \rho_n \sigma dl$, where ρ_n is the number density of electrons and dl is the length traversed σ is the scattering cross-section, determined using the Klein–Nishina formula

$$\sigma = \frac{2\pi r_e^2}{x}\left[\left(1-\frac{4}{x}-\frac{8}{x^2}\right)\ln(1+x^2)+\frac{1}{2}+\frac{8}{x}-\frac{1}{2(1+x)^2}\right]$$

where $x = \frac{2E}{mc^2}\gamma(1-\mu\frac{v}{c})$. Here, $r_e = e^2/mc^2$ is the classical electron radius and m is the mass of the electron.

The electrons are assumed to have a relativistic Maxwell–Boltzmann distribution of momentum. If $\boldsymbol{p} = \gamma m \boldsymbol{v}$, with $\gamma = (1-\frac{v^2}{c^2})^{-1/2}$ and $\mu = \hat{\boldsymbol{\Omega}}\cdot\hat{\boldsymbol{v}}$, the number density of electrons between momentum $\boldsymbol{p}$ and $\boldsymbol{p}+d\boldsymbol{p}$ is given by (PSS83)

$$dN(\boldsymbol{p}) \propto \exp[-(p^2c^2+m^2c^4)^{1/2}/kT_e]d\boldsymbol{p}. \quad (20)$$

Based on the scattering cross-section obtained, the optical depth is calculated. If $\tau > \tau_c$, we allow the photon to scatter and assign a new direction based on its energy. A new random τ_c is generated and the process is continued till the photon leaves the system under consideration. Details of the procedure are given in PSS83.

We continue the simulations for all the nine cases listed in Table 1. The angle θ_*, number density n_{ce} and average temperature $T_e(\tau_0)$ were all derived from other parameters. Inclusion of the compression ratio (R_{comp}) and mass of the star (M_{NS}) would make the number of independent parameters to be seven. For our theoretical investigations in this paper, we did not focus on the reduction of the number of parameters in this work, but we can further reduce it by interrelating CENBOL properties from fundamental equations. We vary $\dot{m}_d$ and $\dot{m}_h$ independently and determine the rest of the parameters either using observational facts or through the formulae derived in Section 3. This has been discussed in Section 5.

4.2 Photoelectric absorption

Photoelectric effect due to gases present in the interstellar media (ISM) is the most significant cause of absorption of photon, in the domain of energy we are considering in this paper. Depending on the degree of absorption, the observed spectra can be largely modified between the energies 0.03–10 keV (Morrison & McCammon 1983). We have used the standard formula for photoelectric cross-section

$$\sigma(E) = 4\alpha\sqrt{2}z^5 8\pi\frac{r_e^2}{3}\left[\frac{m_e c^2}{E}\right]^{3.5} \text{cm}^2. \quad (21)$$

An exponential absorption model was used, following the 'wabs' model used in XSPEC, which can be written as

$$M(E) = \exp(-n_H\sigma(E)), \quad (22)$$

where n_H is the equivalent column density of hydrogen in ISM along the observational direction.

In Figs 6–8, the dotted lines show our derived spectra before the interstellar absorption and solid lines show the spectra after absorption. For the cases C1–C9, $n_H = 4.0\times10^{22}$ cm^{-2} was chosen for concreteness.

4.3 Effects of cooling

We focus on the cases when the CENBOL has temperature up to 25 keV, and the accretion rates are not too high ($\leq\dot{M}_{Edd}$). In the flaring branches, however, the observed spectra show the Comptonized spectrum of to extend beyond 200 keV, pointing towards a hotter outer CENBOL. In order to check this effect of cooling, we take the case of comparatively hotter central temperature ($T_{CE} = 250$ keV), and vary the accretion rates to observe the effects of cooling due to Comptonization. In the scenario when cooling is efficient, the static background temperature distribution should be modelled by the modified temperature, rather than the unmodified thick disc distribution. However, the spectra of those cases are not discussed any more as the Comptonized spectra of the disc is well understood in the cases of black hole under the TCAF paradigm.

First, we project the entire 3D simulation region on to an axisymmetric cylindrical grid, for which the thick disc distributions are used. The number density of electron at each grid location (ir, iz), which corresponds to the position (R, z), is given by $n_e(ir, iz)$. Assuming a torus, for axisymmetric system, the total number of electrons within that volume is given by $dN_e(ir, iz)$

$$dN_e(ir,iz) = 2\pi R n_e(ir,iz)dRdz, \quad (23)$$

where dR and dz are the grid sizes in R and z-directions, respectively.

Depending on the actual photon flux and the number of bundles of photons injected, a weightage can be assigned to each bundle. Let the weightage for i^{th} packet be f_W^i. For a completely relativistic hydrogen plasma, the total thermal energy of all the electrons in the torus with temperature $T_e(ir, iz)$ is given by

$$3k_B T_e(ir,iz)dN_e(ir,iz) = 6\pi k_B R T_e(ir,iz)n_e(ir,iz)dRdz. \quad (24)$$

If the i^{th} packet of photon undergoes Compton scattering at the position (ir, iz) on the grid gaining (or losing) energy ΔE^i, then the final temperature $k_B T_e'(ir, iz)$ after all the photons have left the system, can be written as

$$k_B T_e'(ir,iz) = k_B T_e(ir,iz) - \frac{\sum_{i=1}^{i_{max}} \Delta E^i f_W^i}{3dN_e(ir,iz)} \quad (25)$$

where $i_{max} \sim 10^8$.

We divide the CENBOL into two domains of equal optical depth, calculated along the equatorial plane. If the total optical depth of the CENBOL is τ_0, the region up to $\tau = \tau_0/2$ from the NBOL (or the shock location X_s) is the cloud 'visible' to the NBOL (or the KD), which would produce effectively the same number of scatterings. We determine the average temperature based on the method specified in equation (13), for both the cases, to study the effect of cooling of the CENBOL, by the NBOL and by the disc. This is just to find out the two temperatures in the two halves, which Seifina et al. (STF13, STSS15) and TSS14 found in their work by fitting COMPTB1 and COMPTB2, respectively. The results of this excercise is shown in Fig. 10(a)–(d).

5 RESULTS

The photons are collected outside a sphere of radius R_{out} where they leave our system. They are binned according to their energy, angle of observation, the original location of emission (NBOL or KD) and the number of scatterings each of them suffered. We generate the output spectra from these information.

We first report variation of spectra with respect to the number of scatterings in CENBOL. A considerable fraction of the seed photons emitted are intercepted by CENBOL. This interception and subsequent Comptonization depend on the density and temperature along the path of the photon. These parameters are, however, governed by the accretion rates. In case of a black hole, matter is advected in through the event horizon and the efficiency of radiation

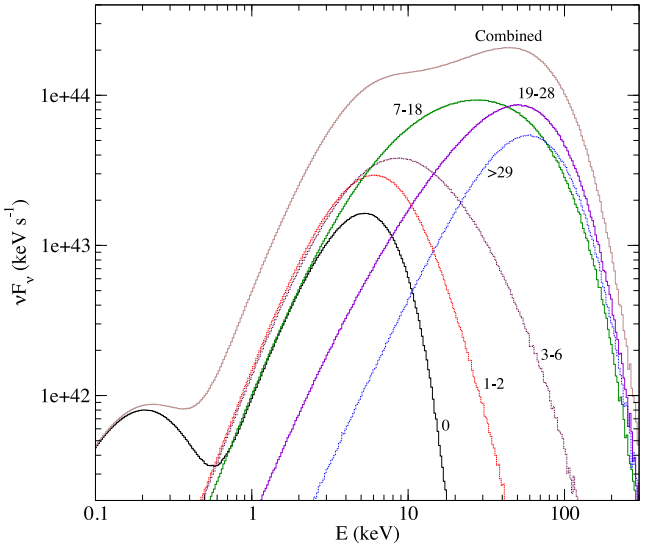

Figure 3. Evidence of hardening of spectra with the number of scattering. The seed photons are emitted from the NBOL and KD and are Comptonized by CENBOL. Here, halo accretion rate $\dot{m}_{\rm h}$ is 0.5 and disc accretion rate is $\dot{m}_{\rm d}$ is 0.1. The photons are binned based on the number of scatterings they underwent before emerging out of the system. The binning was done for 0, 1–2, 3–6, 7–18, 19–28, 29 or higher number of scatterings. These numbers are written beside the corresponding curves to give an idea of how variously scattered photons contribute to the spectra. The combined spectrum is also plotted.

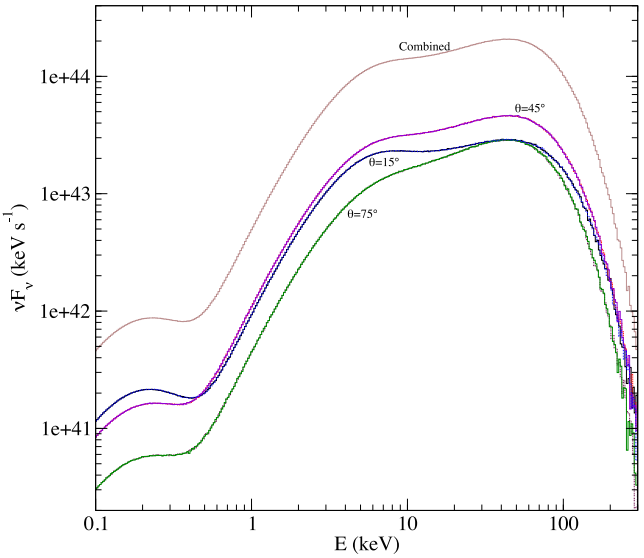

Figure 4. Evidence of hardening of spectra with the observing angle. The seed photons are emitted from the NBOL and KD and are Comptonized by CENBOL. Here, halo accretion rate $\dot{m}_{\rm h}$ is 0.5 and disc accretion rate is $\dot{m}_{\rm d}$ is 0.1. Photons are binned according to the direction of observation. All the angles are measured with respect to the rotation axis (z-axis). The number beside each plot shows the corresponding average angle for each bin (°).

is around 6 per cent, leading to a large, though notional, upper limit ($\sim 16\ \dot{M}_{\rm EDD}$) of the KD accretion rate. In the case of an NS, the hard surface ensures the stopping of the flow at the surface and the radiation decreases the upper limit of maximum acceptable accretion rate. For our calculations, we have strictly kept the upper limit at $1.0\ \dot{M}_{\rm EDD}$. The density is, thus, lower than that around a black hole, leading to a lower number of scatterings of the photons emitted by the KD. The seed photons emitted by the NBOL, however, are exposed to the densest region of CENBOL first and that leads to a significant number of scattering. As a result, the contribution to hard X-Rays from seed photons that originated from the disc is smaller compared to those emitted from NBOL and the overall spectra, in hard states, is expected to be softer than the hard state spectra of a black hole. The observational differences are reported by Gilfanov (2010). We plot the variation of the combined spectra for the case C3 (from Table 1), with respect to the number of scattering in Fig. 3. The binning is done for scattering number 0 (no scattering), 1–2, 3–6, 7–18, 19–28, 29 and above. The overall spectra are also drawn. What is clear is that the photons from the KD are not scattered much. The lower number of scatterings (including those emitted without scattering) of NBOL photons produced the first hump at around 6 keV, while higher number of scatterings that are effectively close to the hot region of CENBOL (i.e. centre), produce the hump at ∼45 keV.

The spectral properties of any compact object in space, be it an NS or a black hole, depend on the inclination angle between the objects line of sight and direction in which the photon is emitted. In the presence of an accretion disc, which emits photons maximally along the local normal, the received flux is maximum when the disc is seen end-on and minimum when seen edge-on. In order to check the validity of any spectral model, it has to be compared with observational data and angle dependency of spectra is to be studied to achieve that. We plot the variation of spectra when the photons are binned with respect to the average direction of observation, viz., 0°–30°, 30°–60°, 60°–90°. In the system, both the photon sources emit photons symmetrically with respect to the equatorial plane or the angle $\theta = 90°$. The structure of CENBOL has the same symmetry as well. As no advection velocity or spin effects are included to derive CENBOL properties, the emergent Comptonized spectra are expected to have the symmetry of the system. Thus in Fig. 4, we indicate the spectra of photons along the average bin angle in the bins of the first quadrant only. The peak flux of unscattered spectra from the KD decreases with increase of angle θ. In case of the radiation from NBOL, the peak flux direction is decided by the peaks of the double Gaussian distribution of emitted flux used in the simulation (Case C3) are along $\theta_{\rm P}^{-} = 54.^{\circ}94$ in the first quadrant. The flux is modulated further due to the interception by CENBOL. The geometry of the post-shock region blocks the escape of unscattered photons emitted at high values of θ. This is reflected in Fig. 5(a). The low energy peaks are due to photons emitted from the KD and the high energy peaks are formed by photons from NBOL. The scattered photons, however, with the increase of the number of scatterings, lose their initial directional distribution and are re-distributed almost isotropically. Although, the presence of the disc and the NS, both of which recapture scattered photons, lowers the number of photons received at around angle $\theta = 90°$. The net flux is highest at ∼45° since the flux of NBOL is high at $\theta = \theta_{\rm P}^{-} = 54.^{\circ}94$ and still has some direct effect. The remnant effect of the double Gaussian enhances the flux along this direction. The Fig. 5(b) showcases this.

As shown in the context of black holes (CT95; GCL09), a rise of halo accretion rate for a given disc accretion rate, makes the spectrum harder. Because of its hard surface, the upper limit of accretion rate for NSs is also much lower than that for black holes. This restricts the density of post-shock region leading to relatively softer spectra when compared to the spectra of black holes. Of course, a major factor is the abundance of seed photons from NBOL itself.

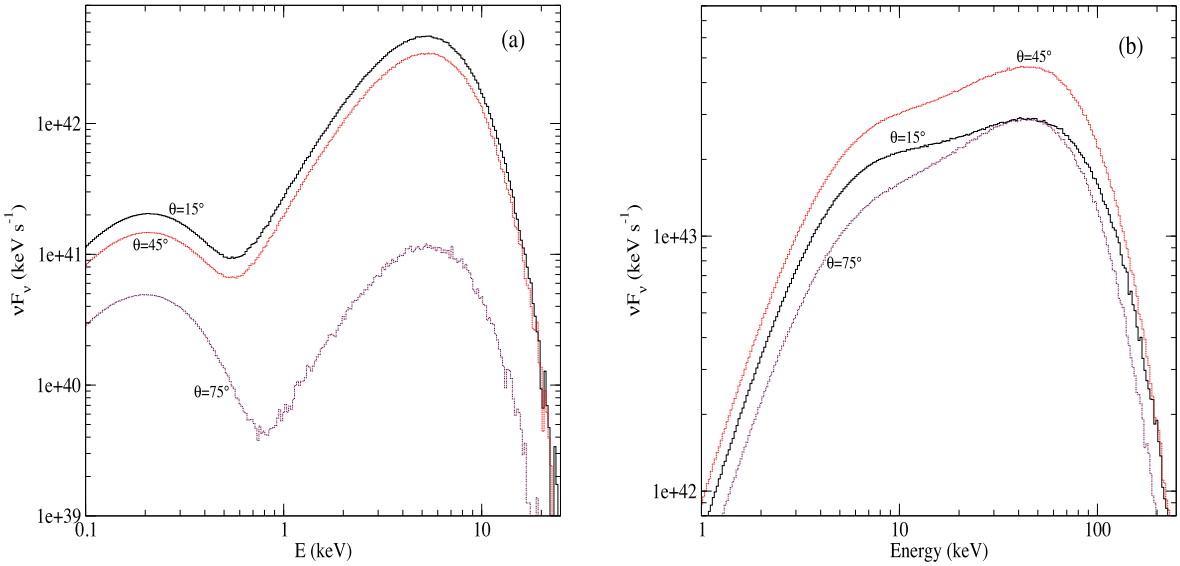

Figure 5. Evidence of hardening of spectra with the observing angle. The seed photons are emitted from the NBOL and KD and are Comptonized by CENBOL. The flow parameters are for Case C3 of Table 1. The photons are binned according to the direction of observation. All the angles are measured with respect to the rotation axis (z-axis). The numbers beside each plot shows the corresponding average angle bins (in degrees). In panel (a), only the photons that escape without being scattered are binned. The angle dependency arises out of the injection direction and geometry of CENBOL. In panel (b), all the photons that underwent at least one scattering are clubbed together.

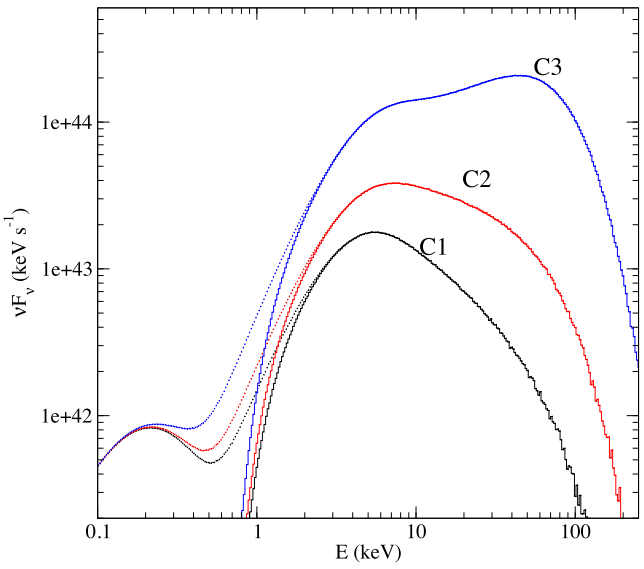

Figure 6. The variation of combined spectra from NBOL, KD and the Comptonized photons as $\dot{m}_{\rm h}$ is varied from 0.1, 0.2 and 0.5. Here, $\dot{m}_{\rm d} = 0.1$ (Cases C1–C3). The dotted lines show our computed spectra as are emitted from the disc, while the solid lines show our spectra after absorption through ISM as they reach us. Here, we used photoelectric absorption due to hydrogen atoms, with $n_{\rm H} = 4 \times 10^{22}$ cm^{-2}. The cases C1–C3 are shown in black, red and blue, respectively (online version).

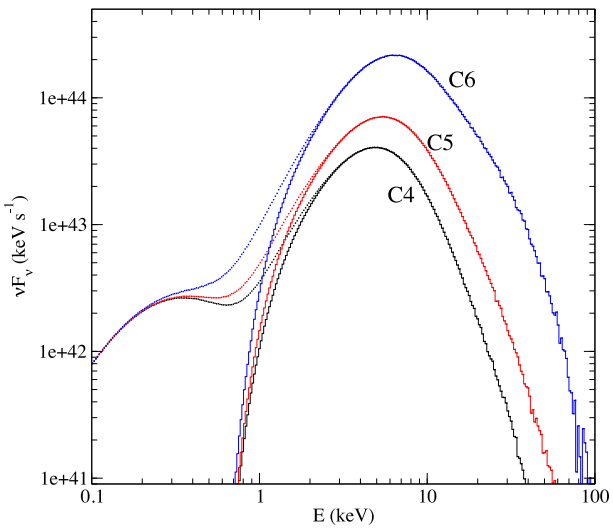

Figure 7. Variation of combined spectra from NBOL, KD and the Comptonized photons as $\dot{m}_{\rm h}$ is varied from 0.1, 0.2 and 0.5. Here, $\dot{m}_{\rm d} = 0.2$. (Cases C4–C6). Dotted lines show our computed spectra as are emitted from the disc, while the solid lines show our spectra after absorption through ISM as they reach us. Here, we used photoelectric absorption due to hydrogen atoms, with $n_{\rm H} = 4 \times 10^{22}$ cm^{-2}. The cases C4–C6 are shown in black, red and blue, respectively (online version).

Figs 6–8 show how, in each case, the spectrum is affected by the increase of the halo accretion rate. In order to account for the cooling due to photons emitted by disc, we decreased the temperature of CENBOL self-consistently with the increase of $\dot{m}_{\rm d}$ (see Table 1). In Fig. 8, the spectrum is roughly a superposition of two blackbody emissions in each of the three cases. In Fig. 7, the Compton up-scattering slightly modifies the spectra but they still remain in typical soft states. In Fig. 6, where $T_{\rm CE} = 25$ keV, the spectrum changes from soft to hard with the increase of $\dot{m}_{\rm h}$. We take the linear domain of the log (νF_ν) versus log (E) curves plotted in logarithmic scales, if present, and try to fit the data with a power law having spectral index α ($\nu F_\nu \sim E^{-\alpha}$). The spectral index α, has the values 0.926, 0.357 and −0.239 as $\dot{m}_{\rm h}$ takes the values 0.1, 0.2 and 0.5, respectively. The indices are calculated from the best fit of the spectra in the energy range 10.0–20.0 keV. We have shown the theoretical spectra for cases C1–C9, in Figs 6–8, with dotted lines and the spectra after absorption through ISM are plotted with solid

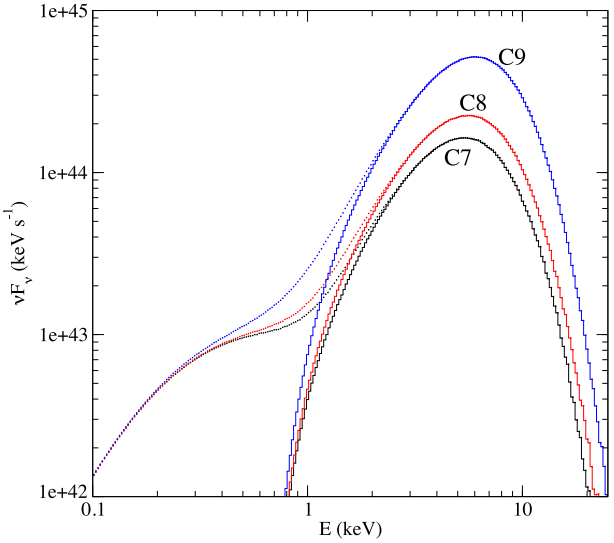

Figure 8. Variation of combined spectra from NBOL, KD and the Comptonized photons as $\dot{m}_h$ is varied from 0.1, 0.2 and 0.5. Here, $\dot{m}_d = 0.5$. (Cases C7–C9). Dotted lines show our computed spectra as are emitted from the disc, while the solid lines show our spectra after absorption through ISM as they reach us. Here, we used photoelectric absorption due to hydrogen atoms, with $n_H = 4 \times 10^{22}$ cm^{-2}. The cases C7–C9 are shown in black, red and blue, respectively (online version).

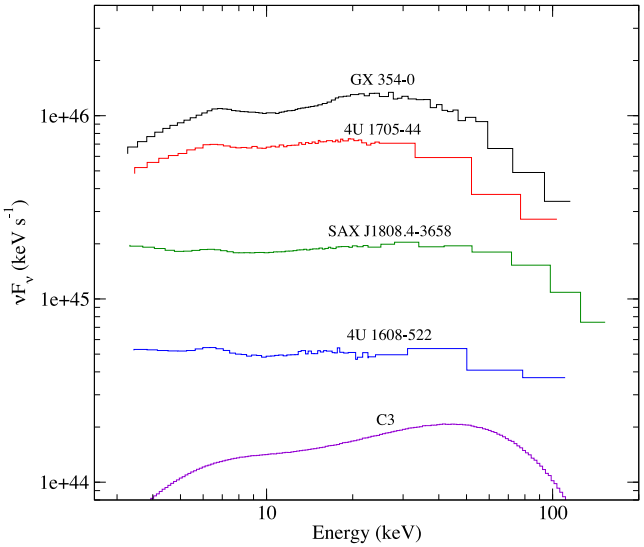

Figure 9. The spectra of a few weakly magnetized NSs, namely, 4U 1705-44, 4U 1608-522, SAX J1808.4-3658 and GX 354-0. For comparison, we put the spectrum of Case C3 (without the iron line emission) of our simulation to show that we generally reproduce the features. These observed spectra were obtained by *RXTE* observations and are adapted from Gilfanov (2010).

lines. Cases C1, C4, and C7 are in black, C2, C5, and C8 are in red and C3, C6 and C9 are in blue (online version). Please note that unlike some models (e.g. White et al. 1986; Mitsuda et al. 1989), we do not give emphasis on the NBOL temperature or the decrease of the total luminosity. Rather, our harder states are primarily achieved due to hotter CENBOL with higher advective halo rates.

The absorption due to the presence of interstellar medium modifies the low energy spectra considerably. In the hard states, when the disc accretion rate is low, the multicolour blackbody component is hardly observed as a separate peak due to the heavy absorption below 1 keV. This was reflected in the Figs. 6–8. After these considerations, the spectra corresponding to Case C3, looks similar to hard state spectra of NSs (see fig. 9, adapted from Gilfanov 2010). The spectrum of NSs in hard states is relatively softer than those of black holes, because of the upper bound of maximum accretion rate. The spectra of a number of weakly magnetized accreting stars were chosen to highlight that fact in Fig. 9. They also have the characteristic iron line emission around 6.5 keV. Apart from that feature, the observed spectra of NSs, as reported in Gilfanov (2010), are similar to our Case C3, which does not include the iron line emission. It can also be concluded that the variation of the parameters of our model, for example, T_{NS}, T_{CE}, X_s, R_{comp}, $\dot{m}_d$ *and* $\dot{m}_h$ can reproduce the observed spectra when suitable normalization is used. In this paper, we report only the variation of spectra with accretion rates. The variation of other parameters and comparison with observed spectra would be reported elsewhere.

To check the variation of the effective geometry of the Compton cloud, CENBOL, as discussed in Section 4.3, we varied the accretion rates and the central temperature T_{CE} of the CENBOL and observed how the Compton scattering changed the temperature profile. For T_{CE} values reported in Table 1, the effect was insignificant and are not shown here. But, the cooling mechanism is more prominent when the central temperature is high. To showcase these effects, we chose the case where $T_{CE} = 250$ keV and $X_s = 46.8 r_S$.

We are reporting four cases here where the halo accretion rate is varied from 0.3 to 0.9, as shown in Fig. 10(a)–(d). As the accretion rates increase, so does the temperature of the NBOL, the cooling is more efficient. Not only that, the effective temperature closer to NBOL decreases more than the one nearer to the disc, as can be seen from the shifting of the peak towards the disc in Fig. 10(a)–(d). From these figures, one can see that the effective geometry of the CENBOL is similar to the ones proposed by TSS14 for the flaring branches. The temperature of cloud near the disc are in between ∼30 and ∼65 keV for the cases studied here, which are in the same ballpark figure as found from COMPTB model analysis in TSS14 and STSS15.

6 DISCUSSIONS AND CONCLUSIONS

In the literature, much studies have been done of the advective flows around black holes and their spectral properties. These solutions typically consist of two components, with a KD flanked vertically by an advective component. Moreover, the inner part of the advective component forms a centrifugal barrier and the post-barrier region (CENBOL) was found to behave as the Compton cloud producing typically the power law with exponential cut-off. CT95 has demonstrated that the spectrum changes from soft to hard as the relative importance of accretion rate of the Keplerian component vis-à-vis the accretion rate of the halo is decreased. Since the segregation of the advective flow into a Keplerian and sub-Keplerian components could take place very far out, there is no a priori reason why an NS accretion could not also manifest into the same two types of components, especially that very far away the flow has not knowledge of the nature of the compact object.

In this paper, we used the successful paradigm of TCAF in the context of a weakly magnetized NS accretion flow. The flow properties were changed on the NS surface due to modification of the inner boundary condition and a blackbody emitting NBOL is created on the NS surface, in addition to the CENBOL in TCAF. Due to the extra source of seed photons, the CENBOL became cooler

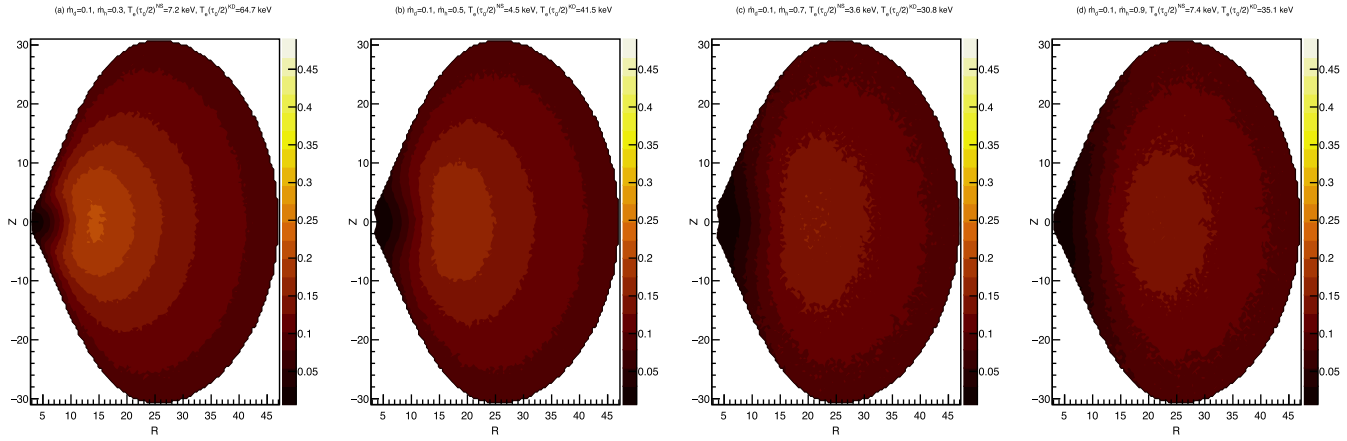

Figure 10. The temperature contours after Compton cooling, from the simulation (for initial $T_{CE} = 250.0$ keV, $X_s = 46.8 r_S$). The temperatures are written in dimensionless unit (kT_e/mc^2). From the left- to right-hand side, the halo accretion rate is increased from 0.3 to 0.9. For panel (a)–(c), with the increase of $\dot{m}_h$, the temperature of CENBOL closer to NBOL, $T_e(\tau_0/2)^{NS}$ decreased from 7.2 to 3.6 keV. The temperature of CENBOL closer to disc, $T_e(\tau_0/2)^{KD}$, also decreased from 64.7 to 30.8 keV, but remain greater than the corresponding $T_e(\tau_0/2)^{NS}$. In the case of panel (d), where the angle θ_* was $\pi/2$, a large fraction of blackbody photons escaped the system without scattering and hence the effect of cooling, although present, is less than the case panel (c). The modified contours show the effective region of Compton scattering and are similar to the proposed geometry of TSS14.

easily and the spectra appeared to be softer for the same input flow parameters. The behaviour of CENBOL is similar to the Compton cloud invoked phenomenologically by TSS14. In our analysis, we restricted our studies within one Eddington rate. However, the general conclusion that the spectrum is hardened with the increase in halo accretion rate remains valid.

The resulting spectrum has several features arising out of the specific flux emission properties of the normal boundary layer, namely, NBOL. The radiation dynamics of NBOL with KD reveals (IS99) that the maximum flux emitted from the NBOL may not be really along the equatorial plane, but from an angle (θ_*). This, together with the fact a CENBOL intercepts more photons from the NBOL than the Keplerian component, produces double hump patterns in the spectra. Photons from NBOL are inverse Comptonized more efficiently and thus dictate the spectra to a greater extent. We also studied how the spectra would change with the observing angle and found that with increasing inclination angle, the spectra are indeed hardened, a result also valid for black hole accretion (GCL09; GGCL10). However, unlike a black hole accretion, in the present scenario, the radiation could be maximum at an intermediate viewing angle (e.g. ∼45 in Fig. 4) and not necessarily along the polar axis.

The observed spectra from NS candidates, especially those which have weak magnetic fields, are found to have similar shapes as found in this paper thus confirming the general idea that TCAF can be used in the spectral study of NSs as well. For instance, the hard spectra of case C3 (Fig. 6) are similar to those of several NSs (Gilfanov 2010). Similar results have also been reported by Lin, Remillard & Homan (2007). Thus, the motivation of our exercise to check if the studies of the black hole and NS spectra could be carried out under a common framework is well justified.

Chakrabarti (1997) expanded CT95 work on TCAF to establish that the advective component of accretion (the sub-Keplerian halo) is essential to produce the hotter CENBOL. Otherwise, if the TL is produced solely from the KD and its optical depth and temperature were calculated self-consistently, the Comptonization would be sufficient to cool it down. Otherwise, one can use the latter quantities as free parameters without explicit use of the second component as in TSS14, who reproduce the spectra very satisfactorily. In this paper, we kept in mind the inter-relationship among the flow parameters and thus nine cases have been put in three main groups of increasing Keplerian accretion rate. Our NBOL cools the inner CENBOL rapidly. So in a way, the CENBOL behaves like the TL of TSS14.

It has been reported from observations that the photon index of COMPTB model for the νF_ν versus $h\nu$ spectra reaches a saturation value of $\Gamma \sim 2$, for the Comptonized spectra of an NS. The spectra from the disc's Comptonized components, however, show no such saturation in general. In ST11 and ST12, the spectra were fitted with *Bbody* + *COMPTB* + *Gaussian*, where the Bbody was related to the disc emission. In STF13, two *COMPTB* + *Bbody* components were used, where both the photon indices show stability around the value 2. In TSF13, the cloud temperature was seen to vary from 2.9 to 21 keV without any significant change in spectral slope of COMPTB spectra due to NS, but the normalization decreased by a factor of 8. TSS14 and STSS15 have shown the saturation of spectral index of COMPTB (for NS only) with respect to the variation of the temperature of the Compton cloud. The second COMPTB component showed a two-phase behaviour: In HB-NB, the photon index was around 2, but in FB, the photon index decreased and had values $1.3 < \Gamma < 2$. It was stated that the spectrum at the FB is determined by high radiation pressure from the NS surface. Burke, Gilfanov & Sunyaev (2017) also reported the constancy of Comptonization parameters, which reflects saturation of photon index at around $\Gamma \sim 2$. In all these cases, the illumination factor f, that controls the amount of Comptonization by the Compton cloud, underwent significant changes, which shows that the geometry or the size of the Compton cloud was changing with spectral states. In STS16, it was shown that the second COMPTB component (for the Comptonized spectra of the disc) showed variations around $\Gamma \sim 2$. Γ went below 2 when the disc temperature is reduced from 1.1 to 0.8 keV, implying an expansion of Compton cloud. A simultaneous increase of the cloud temperature (of the outer part) was also observed. These phenomenological results can be very well understood by varying halo accretion rate, which appears to be the key controlling factor here. With the increase of $\dot{m}_h$, more hot electrons are supplied, resulting in the expansion of CENBOL and spectral hardening (CT95, GGC14). We explore the variation

of spectra with the halo accretion rate for such cases. The results are consistent with observed results.

The proposed geometry of the Compton cloud in TSS14, for the flaring branch shows a hotter outer TL and a cooler inner TL. When we consider the effects of cooling within the Monte Carlo simulation and modify the temperature of the CENBOL, a similar profile is obtained, as shown in Fig. 10(a)–(d). The peak of the distribution shifts towards the disc as accretion rate is increased, for a given initial set of temperature and shock location. The temperatures obtained by us are also consistent with the observed values as reported in TSS14 and STSS15.

Recently, the TCAF solution has been used to fit spectra of several black hole candidates and at the same time to extract physical flow properties and the mass of the compact object (Molla et al. 2017, 2016; Bhattacharjee et al. 2017, and references therein). In near future, we plan to extract physical flow parameters on to NSs as well. Similarly, we are also extending the time-dependent studies of TCAF flow with radiative transfer in order to understand real reason for the high and low-frequency quasi-periodic oscillations in NS systems. In a future work, we will compare the spectral fits using our model and fits obtained using COMPTB model.

ACKNOWLEDGEMENTS

We would like to the thank the referee Dr Lev Titarchuk for bringing to our attention the Comptonizing properties of their TL.

REFERENCES

Barret D., 2001, Adv. Space Res., 28, 307
Barret D., Olive J.-F., 2002, ApJ, 576, 391
Bhattacharjee A., Chakrabarti S. K., Banerjee A., 2016, Proceedings of the 41st COSPAR Scientific Assembly at Istanbul, Can a neutron star also have a two component advective flow? p. 189
Bhattacharjee A., Banerjee I., Banerjee A., Debnath D., Chakrabarti S. K., 2017, MNRAS, 466, 1372
Burke M. J., Gilfanov M., Sunyaev R., 2017, MNRAS, 466, 194
Chakrabarti S. K., 1985, ApJ, 288, 1
Chakrabarti S. K., 1989, MNRAS, 240, 7 (C89)
Chakrabarti S. K., 1990, Theory of Transonic Astrophysical Flows. Scientific Press, Singapore (C90)
Chakrabarti S. K., 1996, ApJ, 464, 66d4 (C96)
Chakrabarti S. K., 1997, ApJ, 484, 313
Chakrabarti S. K., 2016 inRuffini R., Jantzen R., Bianchi M., eds, Proceedings of the 14th Marcel Grossman Meeting at Rome, Study of Accretion Processes Around Black Holes becomes Science: Tell Tale Observational Signatures of Two Component Advective Flows. World Scientific Press, Singapore, In press, (arXiv:1604.05955)
Chakrabarti S. K., Molteni D., 1995, MNRAS, 272, 80
Chakrabarti S. K., Sahu S. A., 1997, A&A, 323, 382 (CS97)
Chakrabarti S. K., Titarchuk L. G., 1995, ApJ, 455, 623 (CT95)
Chakrabarti S. K., Wiita P. J., 1993, ApJ, 411, 602
Chakrabarti S. K., Jin L., Arnett W. D., 1987, ApJ, 313, 674 (CJA87)
Chatterjee D., Debnath D., Chakrabarti S. K., Mondal S., Jana A., 2016, ApJ, 827, 88
Debnath D., Chakrabarti S. K., Nandi A., Mandal S., 2008, BASI, 36, 151
Debnath D., Chakrabarti S. K., Nandi A., 2010, A&A, 520, 98
Debnath D., Chakrabarti S. K., Mondal S., 2013a, ASICS, 8, 85
Debnath D., Chakrabarti S. K., Nandi A., 2013b, AdSpR, 52, 2143
Di Salvo T., Stella L, 2002, in Goldwurm A., Neumann D., Tran Thanh Van J. eds, Proc. of the XXII Moriond Astrophysics Meeting, The Gamma-Ray Universe. The Gioi Publishers, Vietnam, preprint (arXiv:astro-ph/0207219)
Dutta B. G., Chakrabarti S. K., 2016, ApJ, 828, 101
Farinelli R., Titarchuk L., 2011, A&A, 525, A102 (FT11)
Farinelli R., Titarchuk L., Paizis A., Frontera F., 2008, ApJ, 680, 602
Garain S. K., Ghosh H., Chakrabarti S. K., 2014, MNRAS, 437, 1329 (GGC14)
Ghosh H., Chakrabarti S. K., Laurent P., 2009, IJMPD, 18, 1693 (GCL09)
Ghosh H., Garain S. K., Chakrabarti S. K., Laurent P., 2010, IJMPD 19, 607 (GGCL10)
Gilfanov M., 2010, in Belloni T. ed.,The Jet Paradigm. Lecture Notes in Physics, Vol. 794. Springer-Verlag, Berlin Heidelberg, p. 17 (G10)
Gilfanov M. R., Sunyaev R. A., 2014, Physics-Upsekhi, 57, 377 (GS14)
Giri K., Chakrabarti S. K., 2013, MNRAS, 430, 2836 (GC13)
Giri K., Garain S. K., Chakrabarti S. K., 2015, MNRAS, 448, 3221 (GGC15)
Haardt F., Maraschi L., 1993, ApJ, 413, 507
Inogamov N. A., Sunyaev R. A., 1999, Astron. Lett., 25, 269 (IS99)
Jana A., Debnath D., Chakrabarti S. K., Mondal S., Molla A. A., 2016, ApJ, 819, 107
Lin D., Remillard R. A., Homan J., 2007, ApJ, 667, 1073
Mitsuda K. et al., 1984, PASJ, 36, 741
Mitsuda K., Inoue H., Nakamura N., Tanaka Y., 1989, PASJ, 41, 97
Molla A. A., Debnath D., Chakrabarti S. K., Mondal S., Jana A., 2016, MNRAS, 460, 3163 (M16)
Molla A. A., Chakrabarti S. K., Debnath D., Mondal S., 2017, ApJ, 834, 88 (M17)
Molteni D., Lanzafame G., Chakrabarti S. K., 1994, ApJ, 425, 161
Molteni D., Sponholz H., Chakrabarti S. K., 1996, ApJ, 457, 805
Mondal S., Chakrabarti S. K., 2013, MNRAS, 431, 2716 (MC13)
Mondal S., Debnath D., Chakrabarti S. K., 2014, ApJ, 786, 4
Mondal S., Chakrabarti S. K., Debnath D., 2016, Ap&SS, 361, 309
Morrison R., McCammon D., 1983, ApJ, 270, 119
Odaka H., Khangulyan D., Tanaka Y. T., Watanabe S., Takahashi T., Makishima K., 2013, ApJ, 767, 70
Odaka H., Khangulyan D., Tanaka Y. T., Watanabe S., Takahashi T., Makishima K., 2014, ApJ, 780, 38
Paizis A. et al., 2006, A&A, 459, 187
Popham R., Sunyaev R. A., 2001, ApJ, 547, 355 (PS01)
Pozdnyakov L. A., Sobol I. M., Sunyaev R. A., 1983, Astrophys. Space Sci. Rev. 2, 189 (PSS83)
Ryu D., Chakrabarti S. K., Molteni D., 1997, ApJ, 474, 378
Seifina E., Titarchuk L., 2012, ApJ, 747, 99 (ST12)
Seifina E, Titarchuk L, 2011, ApJ, 738, 128; (ST11)
Seifina E., Titarchuk L., Frontera F., 2013, ApJ, 766, 63 (STF13)
Seifina E., Titarchuk L., Shrader C., Shaposhnikov N., 2015, ApJ, 808, 142 (STSS15)
Seifina E., Titarchuk L., Shaposhnikov N., 2016. ApJ, 821, 23 (STS16)
Seon K.-I., Choi C.-S., Nam U.-W., Min K.-W., 1994, JKAnS, 27, 45
Shakura N. I., Sunyaev R. A., 1973, A&A, 24, 337 (SS73)
Smith D. M., Heindl W. A., Markwardt C. B., Swank J. H., 2001, ApJ, 554, L41
Smith D. M., Heindl W. A., Swank J. H., 2002, ApJ, 569, 362
Sunyaev R. A., Titarchuk L. G., 1980, ApJ, 86, 121 (ST80)
Sunyaev R. A., Titarchuk L. G., 1985, A&A, 143, 374 (ST85)
Sunyaev R. A., Truemper J., 1979, Nature, 279, 506 (ST79)
Titarchuk L., Lapidus I., Muslimov A., 1998, ApJ, 499, 315 (TLM98)
Titarchuk L., Seifina E., Frontera F., 2013, ApJ, 767, 160 (TSF13)
Titarchuk L., Seifina E., Shrader C., 2014, ApJ, 789, 98 (TSS14)
White N. E., Peacock A., Hasinger G., Mason K. O., Manzo G., Taylor B. G., Branduardi Raymont G., 1986, MNRAS, 218, 129
Zdziarski A. A. et al., 2003, MNRAS, 342, 355

This paper has been typeset from a TEX/LATEX file prepared by the author.